**Proceedings of ASME Turbo Expo 2014**
**GT2014**
**June 16-20, 2014, Düsseldorf, Germany**

**GT2014-27230**

# MODELING AND ANALYSIS OF TIME-PERIODIC GEARBOX VIBRATION

**Shengli Zhang**
Department of Mechanical Engineering
University of Connecticut
Storrs, CT 06269, USA

**Jiong Tang**
Department of Mechanical Engineering
University of Connecticut
Storrs, CT 06269, USA

**Yu Ding**
Department of Industrial & Systems Engineering
Texas A&M University
College Station, TX 77843, USA

## ABSTRACT

In a modern wind turbine, the gearbox is an expensive and fault-prone subsystem. Currently, condition monitoring, based on comparison of data of healthy baseline measurement and online measurement, followed by feature analysis and decision making, is the main approach of diagnosis and prognosis. Although having been employed in many practical implementations, such methods have limitations. For example, a huge database is needed when operating conditions change and normal variations are significant. Traditionally, first-principle-based modeling of gearboxes is considered very challenging, primarily due to their dynamic characteristics that exhibit time-periodicity and encompass a very wide frequency range. In this research, aiming at achieving the predictive modeling capability, a lumped-parameter model of a two-stage laboratory gearbox testbed is constructed based on the assumed mode method. This model can characterize the gearbox dynamic effects including the time-varying mesh stiffness and backlash. The Floquet theory and harmonic balance method are then applied to analytically investigate the system dynamics, where the eigenvalues of the time-periodic gearbox are extracted and correlated to the spectral analysis results of the time-domain response prediction. This modeling approach and the associated analysis lay down a foundation for establishing hybrid dynamic model of complex gearbox systems which will further be utilized in model-based diagnosis and prognosis.

## INTRODUCTION

Gearboxs have been investigated for decades as important subsystems of transmissions in machineries. The reliability and durability of gearbox systems has always been a challenging issue. For example, while today wind power is one of the fastest growing renewable energy sources around the world, their gearbox subsystems are expensive and fault-prone. As the key issue for all renewable energy utilizations is cost and marketability, a reliable, robust fault detection and diagnosis scheme for gearbox plays a critical role in making the wind power more marketable [1-4]. Currently, condition monitoring, based on comparison of data of healthy baseline measurement and online measurement, followed by feature analysis and decision making, is the main approach of diagnosis and prognosis. The related techniques include vibration analysis, acoustic measurements, oil monitoring, thermography, and visual inspection etc, among which vibration analysis is the most widely applied [5, 6]. The underlying idea of this method is to use vibratory response data measured under the healthy status, rather than model prediction, to facilitate detection of abnormality. Although this school of thoughts has shown promising aspects and been practiced in practical implementations, there are severe limitations. For example, a huge database is needed when operating conditions change and normal variations are significant [6, 7].

Typical gearbox diagnosis and prognosis schemes employ vibration responses and acoustic emissions as information carrier. Obviously, predictive modeling of gearbox vibrations with high model fidelity can help elucidate the underlying physics of various faults and even generate dataset that can be used to classify the faults. Nevertheless, traditionally, first-principle-based modeling and analysis of gearboxes is considered very challenging. Indeed, dynamic modeling of gear system has been pursued, starting from a simple mass-spring model in 1950s [8] and advancing to complex, lumped-parameter non-linear ones [9] or those based on finite element methods [10] nowadays. While finite element modeling can reveal the details of local mechanical behaviors such as gear meshing, the computational cost becomes almost prohibitive when time-domain, system-wide responses are pursued. On the other hand, although system-level, lumped parameter models have the potential to rapidly predict vibration responses over time, the model accuracy is usually questionable and the selection of model parameters is often *ad hoc*. For example, many of the lumped-parameter models treat shafts in a gear system as a series of lumped mass-spring elements [11, 12] that can only mimic one of the shaft's mode shapes whereas other modes are neglected. This limitation severely affects the model fidelity especially for systems operating under varying speed conditions such as the gearbox in a wind turbine.

The fundamental challenges in gearbox modeling include the time-periodicity and that the dynamic responses encompass a very wide frequency range. In this research, we incorporate the assumed mode method (AMM) into the lumped-parameter model of a two-stage laboratory gearbox testbed. In an AMM treatment, the shafts are discretized by using the linear superposition of beam vibration modes within the frequency range of interest. Hence the high-frequency harmonics features and the relative displacement of the gear pairs along the line of action can be evaluated with good accuracy. Moreover, the dynamic effect caused by the bearing stiffness and damping can be involved in the mathematical model conveniently. Meanwhile, the dynamic models of gearbox systems are in general time-varying and nonlinear when mesh stiffness, backlash, and friction etc are introduced [9, 13-16]. To analyze the time-periodicity, some recent studies resort to the Floquet Theory. For example, DeSmith et al [17] applied this theory to analyze the stability of the system. Vaishya and Singh [13] and Singh [18] directly analyzed the time-domain response of the system using the Floquet Theory for single degree-of-freedom (DOF) systems. In this research, we attempt to use the Floquet theory to investigate the dynamic characteristics of a time-periodic multi-DOF system.

The rest of this paper is organized as follows. We first formulate the system-level model of a two-stage laboratory gearbox based on the assumed mode method. The model includes torsional and translation DOFs of the shafts, time-periodic mesh forces as well as the backlash effect. We then explore the usage of the combination of the Floquet theory and the harmonic balance method to evaluate the system dynamic behaviors. We start from using such combination to study a simplified 4-DOF gear pair for demonstration and validation, followed by comprehensive numerical investigations on the laboratory gearbox testbed. Specifically, we compare the spectral analysis results of the time-domain responses and the eigenvalues directly extracted from the time-periodic model. Such correlation can reveal the underlying dynamic characteristics of the resonances and frequency sidebands exhibited in the vibration responses, and can provide basis for developing hybrid model (i.e., combining experimental measurements with numerical prediction) with enhanced fidelity for diagnosis and prognosis.

## MATHEMATICAL MODEL OF THE GEARBOX

Here we consider the setup shown in Figure 1 [11, 16], a two-stage gearbox system. Since the excitations of the system are mainly along the torsional and lateral directions but not the longitudinal direction, the DOFs along the first two directions are considered. Here, AMM is utilized on each shaft along the Y and Z directions, respectively. As shown in Figure 1, there are six rotational DOFs and a number of translational DOFs where the number of translational DOFs depend upon the number of assumed modes employed in AMM discretization. The bearings are modeled as linear stiffness and damping elements along the Y and Z directions on each shaft; the specific parametric values are estimated from vendor's manual and calibrated based on the experimental data.

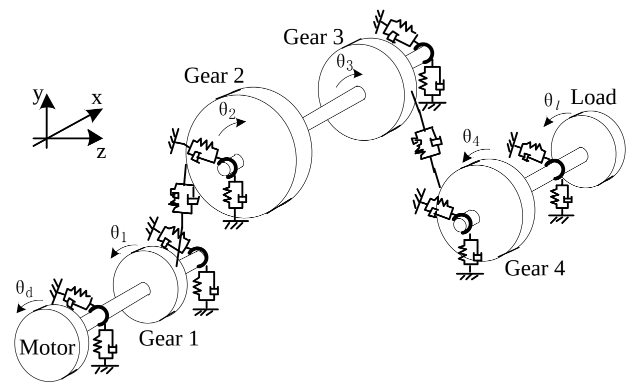


**Figure 1 Dynamic model of the gearbox**

**Torsional DOF considerations**

The equations of motion for the torsional DOFs are given as:

$$
\begin{aligned}
&I_D\ddot{\theta}_D + \mathrm{C}_{t1}\left(\dot{\theta}_D - \dot{\theta}_1\right) + K_{t1}\left(\theta_D - \theta_1\right) = T_D \\
&I_1\ddot{\theta}_1 + \mathrm{C}_{t1}\left(\dot{\theta}_1 - \dot{\theta}_D\right) + K_{t1}\left(\theta_1 - \theta_D\right) = -F_{m1}R_1 \\
&I_2\ddot{\theta}_2 + C_{t2}\left(\dot{\theta}_2 - \dot{\theta}_3\right) + K_{t2}\left(\theta_2 - \theta_3\right) = F_{m1}R_2 \\
&I_3\ddot{\theta}_3 + C_{t2}\left(\dot{\theta}_3 - \dot{\theta}_2\right) + K_{t2}\left(\theta_3 - \theta_2\right) = -F_{m2}R_3 \\
&I_4\ddot{\theta}_4 + C_{t3}\left(\dot{\theta}_4 - \dot{\theta}_L\right) + K_{t3}\left(\theta_4 - \theta_L\right) = F_{m2}R_4 \\
&I_L\ddot{\theta}_L + C_{t3}\left(\dot{\theta}_L - \dot{\theta}_4\right) + K_{t3}\left(\theta_L - \theta_4\right) = -T_L
\end{aligned}
\tag{1}
$$

where $I_D, I_1, I_2, I_3, I_4, I_L$ are the mass moment of inertia for the motor, gear 1, gear 2, gear 3, gear 4 and the load, respectively; $C_{t1}, C_{t2}, C_{t3}, K_{t1}, K_{t2}, K_{t3}$ are torsional damping and stiffness elements of the three shafts, respectively; $F_{m1}$, $F_{m2}$ are the mesh forces acting on the two gear pairs, the detail of which will be explained later; $R_1, R_2, R_3, R_4$ are the "basic circle radii of the four gears.

**Translational DOF consideration**

The AMM applies Lagrange's equations to establish the mathematical model. The physical displacements of the shafts are expressed as linear combinations of the beam assumed modes. For the input shaft transversal vibration, the shaft's deflection $y_1(x,t)$, $z_1(x,t)$, along the Y and Z directions respectively, are described in Eq. (2), in which $n$ eigen-functions (modes) are involved,

$$\begin{cases} y_1(x,t) = \phi_1(x)\, q_{1y}(t) \\ z_1(x,t) = \psi_1(x)\, q_{1z}(t) \end{cases} \tag{2}$$

where $q_{1y} = [a_1 \cdots a_n]^T$, $q_{1z} = [b_1 \cdots b_n]^T$ are the generalized displacements in X-Y and X-Z planes respectively; $\phi_1 = [\phi_{1,1} \;\cdots\; \phi_{1,n}]$ and $\psi_1 = [\psi_{1,1} \;\cdots\; \psi_{1,n}]$ are the corresponding assumed mode shape functions. For a symmetric shaft, it's natural to let $\phi_1 = \psi_1$ whose elements are expressed in Eq.(3) that are derived from free-free boundary conditions of Euler-Bernoulli Beam,

$$\phi_{i,n} = \sin\beta_n x + \sinh\beta_n x + \eta_n(\cos\beta_n x + \cosh\beta_n x) \tag{3}$$

where $\eta_n = \dfrac{\sin\beta_n l - \sinh\beta_n l}{\cosh\beta_n l - \cos\beta_n l}$, $\cos\beta_n l \cdot \cosh\beta_n l = 1$, and $l$ is the length of the shaft.

The equations of motion of the input shaft can then be represented in matrix form as:

$$\begin{bmatrix} \mathbf{M}_{1y}+\mathbf{J}_{1y} & \\ & \mathbf{M}_{1z}+\mathbf{J}_{1z} \end{bmatrix} \begin{bmatrix} \ddot{\mathbf{q}}_{1y} \\ \ddot{\mathbf{q}}_{1z} \end{bmatrix} + \begin{bmatrix} \mathbf{C}_{1y} & \\ & \mathbf{C}_{1z} \end{bmatrix} \begin{bmatrix} \dot{\mathbf{q}}_{1y} \\ \dot{\mathbf{q}}_{1z} \end{bmatrix} + \begin{bmatrix} \mathbf{K}_{1y} & \\ & \mathbf{K}_{1z} \end{bmatrix} \begin{bmatrix} \mathbf{q}_{1y} \\ \mathbf{q}_{1z} \end{bmatrix} = \begin{bmatrix} \mathbf{F}_{1y} \\ \mathbf{F}_{1z} \end{bmatrix} \tag{4}$$

where

$$\begin{aligned} &\mathbf{M}_{1y} = \mathbf{M}_{1z} = \int_0^l \rho A \phi_1^T \phi_1 dx + \sum_{i=1}^{s} m_i \phi_1^T(x_i)\phi_1(x_i) \\ &\mathbf{J}_{1y} = \mathbf{J}_{1z} = \int_0^l \rho I \phi'^T_1 \phi'_1 dx + \sum_{i=1}^{s} J_{di} \phi'^T_1(x_i)\phi'_1(x_i) \\ &\mathbf{C}_{1y} = \mathbf{C}_{1z} = \sum_{i=1}^{t} c_i \phi_1^T(x_i)\phi_1(x_i) \\ &\mathbf{K}_{1y} = \mathbf{K}_{1z} = \int_0^l EI \phi''^T_1 \phi''_1 dx + \sum_{i=1}^{t} k_i \phi_1^T(x_i)\phi_1(x_i) \\ &\begin{cases} \mathbf{F}_{1y} = F_{m1}\sin\alpha \cdot \phi_1^T(x_{g11}) \\ \mathbf{F}_{1z} = -F_{m1}\cos\alpha \cdot \phi_1^T(x_{g11}) \end{cases} \end{aligned} \tag{5}$$

where $A$ is the cross-sectional area of the input shaft, $I$ is the area moment of inertia, $J_{di}$ is the mass moment of inertia with respect to the Y-Y axis of the lumped gear mass $m_i$ located at $x_i$, α=15.5° is the angle between mesh force $F_{m1}$ and Z axis shown in Figure 2, $x_{g11}$ is the location of the gear 1 on the input shaft, and $c_i$ and $k_i$ are the damping and stiffness of the bearings located at $x_i$ respectively [19]. Similarly, equations of motion can be derived for the intermediate and the output shafts, respectively.

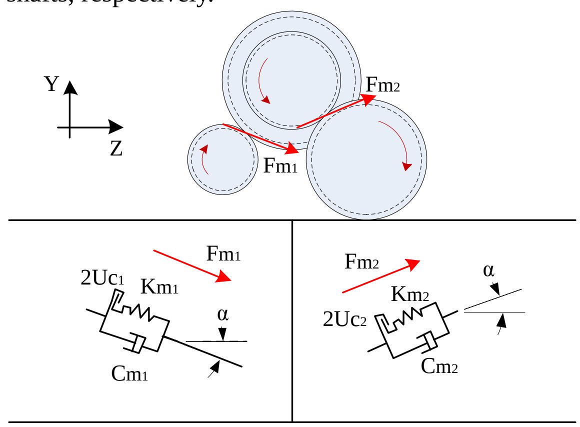


**Figure 2 Mesh forces directions**

**Dynamic mesh forces**

The relative displacements and velocities along the line of action for the two gear pairs are decided by the angular position of the gears and the translational deviations of the shafts. Their equations are given below.

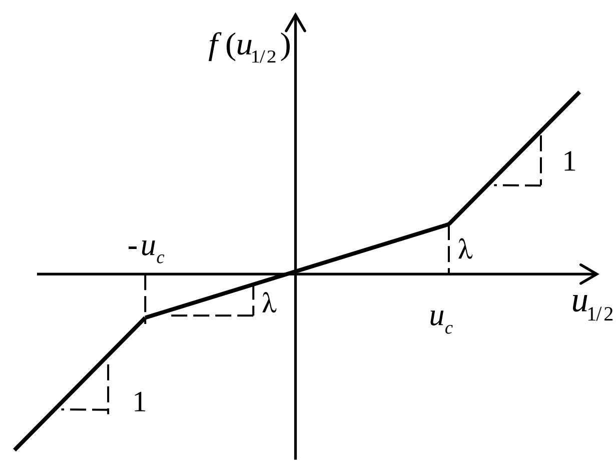


**Figure 3 Nonlinear backlash**

$$\begin{aligned} u_1 = R_1\theta_1 - R_2\theta_2 &- \sin\alpha \cdot \phi_1(x_{g11})\, q_{1y}(t) \\ &+ \cos\alpha \cdot \phi_1(x_{g11})\, q_{1z}(t) \\ &+ \sin\alpha \cdot \phi_2(x_{g21})\, q_{2y}(t) \\ &- \cos\alpha \cdot \phi_2(x_{g21})\, q_{2z}(t) \end{aligned} \tag{6}$$

$$
\begin{aligned}
u_2 = {} & R_3\theta_3 - R_4\theta_4 + \sin\alpha \cdot \phi_2\left(x_{g22}\right)q_{2y}\left(t\right) \\
& + \cos\alpha \cdot \phi_2\left(x_{g22}\right)q_{2z}\left(t\right) \\
& - \sin\alpha \cdot \phi_3\left(x_{g31}\right)q_{3y}\left(t\right) \\
& - \cos\alpha \cdot \phi_3\left(x_{g31}\right)q_{3z}\left(t\right)
\end{aligned}
\tag{7}
$$

$$
\begin{aligned}
\dot{u}_1 = {} & R_1\dot{\theta}_1 - R_2\dot{\theta}_2 - \sin\alpha \cdot \phi_1\left(x_{g11}\right)\dot{q}_{1y}\left(t\right) \\
& + \cos\alpha \cdot \phi_1\left(x_{g11}\right)\dot{q}_{1z}\left(t\right) \\
& + \sin\alpha \cdot \phi_2\left(x_{g21}\right)\dot{q}_{2y}\left(t\right) \\
& - \cos\alpha \cdot \phi_2\left(x_{g21}\right)\dot{q}_{2z}\left(t\right)
\end{aligned}
\tag{8}
$$

$$
\begin{aligned}
\dot{u}_2 = {} & R_3\dot{\theta}_3 - R_4\dot{\theta}_4 + \sin\alpha \cdot \phi_2\left(x_{g22}\right)\dot{q}_{2y}\left(t\right) \\
& + \cos\alpha \cdot \phi_2\left(x_{g22}\right)\dot{q}_{2z}\left(t\right) \\
& - \sin\alpha \cdot \phi_3\left(x_{g31}\right)\dot{q}_{3y}\left(t\right) \\
& - \cos\alpha \cdot \phi_3\left(x_{g31}\right)\dot{q}_{3z}\left(t\right)
\end{aligned}
\tag{9}
$$

where $x_{g21}, x_{g22}$ are the locations of gear 2 and gear 3 on the intermediate shaft, respectively, $x_{g31}$ is the location of the gear 4 on the output shaft.

The non-linear elastic element due to backlash, shown graphically in Figure 3, can be expressed as

$$
f(u_{1/2}) = \begin{cases} u_{1/2} - (1-\lambda)u_c & u_{1/2} > u_c \\ \lambda u_{1/2} & |\, u_{1/2} \,| \le u_c \\ u_{1/2} + (1-\lambda)u_c & u_{1/2} < -u_c \end{cases}
\tag{10}
$$

$$
f(\dot{u}_{1/2}) = \begin{cases} \dot{u}_{1/2} & u_{1/2} > u_c \\ \lambda \dot{u}_{1/2} & |\, u_{1/2} \,| \le u_c \\ \dot{u}_{1/2} & u_{1/2} < -u_c \end{cases}
\tag{11}
$$

where $\lambda$ is the ratio of the second stage stiffness to the first stage stiffness, which indicates the strength of the non-linearity [20], $u_c$ is one half of the backlash Therefore, the mesh forces can be written as:

$$
\begin{cases} F_{m1} = K_{m1} f\left(u_1\right) + C_{m1} f\left(\dot{u}_1\right) \\ F_{m2} = K_{m2} f\left(u_2\right) + C_{m2} f\left(\dot{u}_2\right) \end{cases}
\tag{12}
$$

where $K_{m1}, K_{m2}$ are the mesh stiffness of the first and second gear pair respectively, and $C_{m1}, C_{m2}$ are the mesh damping coefficients. The mesh stiffness can be evaluated through finite element method [10, 21, 22]. The mesh damping are calculated from the damping ratios estimated based on the material properties.

## SYSTEM ANALYSIS BY FLOQUET THEORY

The Floquet theory has been applied extensively to analyze differential equations with periodic coefficients. It was applied to single-DOF spur gear system in [13] and [18] to solve the system response in analytical form. In this section, the Floquet theory application is extended to the multi-DOF system with periodic mesh stiffness. Since no closed-form analytical solutions can be obtained for under-damped, time-varying multi-DOF system, we resort to the combination of the Floquet theory approach and numerical analysis. We further combine the Floquet theory analysis with the harmonic balance method (HBM) to analyze the eigenvalue problems of the linear time-varying system to gain insights.

### System response analysis illustration

In general, the equations of motion of a multi-DOFs gear system can be represented as:

$$
\mathbf{M}\ddot{\mathbf{X}} + \mathbf{C}\dot{\mathbf{X}} + \mathbf{K}\mathbf{X} = \mathbf{F}
\tag{13}
$$

where **M**, **C**, **K** are mass, damping, stiffness matrixes, respectively. **K** is a time-periodic matrix.

In what follows in this section, we first use a simplified periodic mesh stiffness to illustrate the basic procedure. Specifically, we consider piecewise linear mesh stiffness shown in Figure 4. Initially, **C** is assumed to be zero. Hence, Eq.(13) becomes:

$$
\mathbf{M}\ddot{\mathbf{X}} + \mathbf{K}\mathbf{X} = \mathbf{F}
\tag{14}
$$

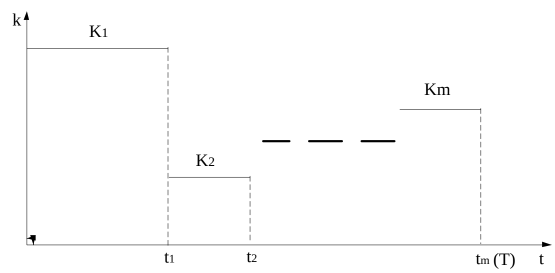


**Figure 4 Periodic mesh stiffness**

For each time-duration within which the stiffness is a constant, we can solve the corresponding eigenvector matrix, denoted as $\mathbf{S}_m$, and decouple the coordinates in the following manner,

$$
\begin{cases} \mathbf{X} = \mathbf{S}_1\mathbf{q}_1, 0 \le t < t_1 \\ \mathbf{X} = \mathbf{S}_2\mathbf{q}_1, t_1 \le t < t_2 \\ \cdots \end{cases}
\tag{15}
$$

which yields

$$
\begin{cases} \ddot{\mathbf{q}}_1 + \mathbf{S}_1^T\mathbf{K}_1\mathbf{S}_1\mathbf{q}_1 = \mathbf{P}_1, 0 \le t < t_1 \\ \ddot{\mathbf{q}}_2 + \mathbf{S}_2^T\mathbf{K}_2\mathbf{S}_2\mathbf{q}_2 = \mathbf{P}_2, t_1 \le t < t_2 \\ \cdots \\ \ddot{\mathbf{q}}_m + \mathbf{S}_m^T\mathbf{K}_m\mathbf{S}_m\mathbf{q}_m = \mathbf{P}_m, t_{m-1} \le t < t_m = T \end{cases}
\tag{16}
$$

where $\begin{bmatrix}\mathbf{P}_1 & \mathbf{P}_2 & \cdots & \mathbf{P}_m\end{bmatrix}^T = \begin{bmatrix}\mathbf{S}_1\mathbf{F} & \mathbf{S}_2\mathbf{F} & \cdots & \mathbf{S}_m\mathbf{F}\end{bmatrix}^T$.

By applying the Floquet theory to Eq.(16), we can obtain a series of transition matrix $\mathbf{\Phi}_i(t,0)$ [13, 18]. Therefore, the solution of Eq.(16) can be obtained as

$$
\mathbf{q}_i(t)=\begin{bmatrix}
\mathbf{\Phi}_i(t-nT,t_{i-1})\mathbf{S}_i^{-1}\cdots \\
\quad \cdot\mathbf{S}_2\mathbf{\Phi}_2(t_2,t_1)\mathbf{S}_2^{-1}\mathbf{S}_1\mathbf{\Phi}_1(t_1,0)\mathbf{S}_1^{-1}\mathbf{X}(nT) \\
+\mathbf{\Phi}_i(t-nT,t_{i-1})\mathbf{S}_i^{-1}\cdots \\
\quad \cdot\mathbf{S}_2\mathbf{\Phi}_2(t_2,t_1)\mathbf{S}_2^{-1}\mathbf{S}_1\mathbf{\Phi}_1(t_1,0)\int_0^{t_1}\mathbf{\Phi}_1^{-1}(\tau,0)\mathbf{P}_1(\tau)d\tau \\
+\mathbf{\Phi}_i(t-nT,t_{i-1})\mathbf{S}_i^{-1}\cdots \\
\quad \cdot\mathbf{S}_2\mathbf{\Phi}_2(t_2,t_1)\int_{t_1}^{t_2}\mathbf{\Phi}_2^{-1}(\tau,t_1)\mathbf{P}_2(\tau)d\tau \\
+\cdots \\
+\mathbf{\Phi}_i(t-nT,t_{i-1})\int_{t_{i-1}}^{t-nT}\mathbf{\Phi}_i^{-1}(\tau,t_{i-1})\mathbf{P}_i(\tau+nT)d\tau
\end{bmatrix}
\tag{17}
$$

Substituting Eq.(17) back into Eq.(15), we can obtain the solution of Eq.(14). For a proportionally damped system that is under-damped, the equations of motion can be re-written as

$$
\begin{cases}
\ddot{q}_1+\tilde{c}_1\dot{q}_1+\tilde{k}_1q_1=P_1, 0\le t<t_1 \\
\ddot{q}_2+\tilde{c}_2\dot{q}_2+\tilde{k}_2q_2=P_2, t_1\le t<t_2 \\
\cdots \\
\ddot{q}_m+\tilde{c}_m\dot{q}_m+\tilde{k}_mq_m=P_m, t_{m-1}\le t<t_m=T
\end{cases}
\tag{18}
$$

We assume here that the system damping is given as $\tilde{c}_i=2\xi_i\sqrt{\tilde{k}_i}\approx 2\xi_i\sqrt{\bar{k}}$ where $\bar{k}$ is the average stiffness [18]. By defining the transformation $q_i=\varphi_i e^{-\tilde{c}_i t/2}\approx\varphi_i e^{-\xi_i t\sqrt{\bar{k}}}$, we can obtain,

$$
\ddot{\varphi}_i(t)+\left[1-\xi_i^2\frac{\bar{k}}{\tilde{k}_i(t)}\right]\tilde{k}_i(t)\varphi_i=P_i/e^{-\xi_i t\sqrt{\bar{k}}}
\tag{19}
$$

Since $\dfrac{\bar{k}}{\tilde{k}_i(t)}\approx 1$, $\xi_i^2$ is negligible for small viscous damping. Hence, the solution to Eq.(18) will be of the same form of that to Eq.(16).

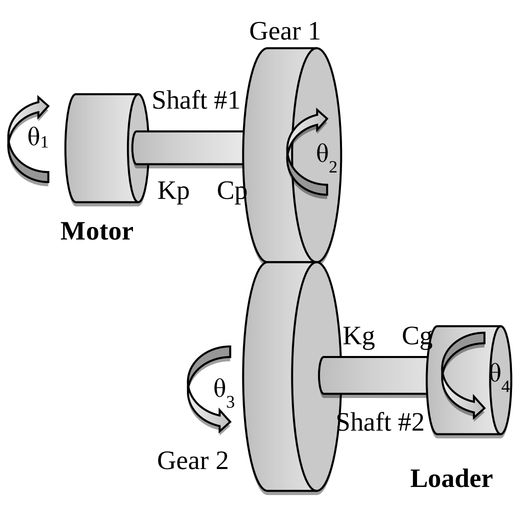


**Figure 5 A 4DOFs gear system**

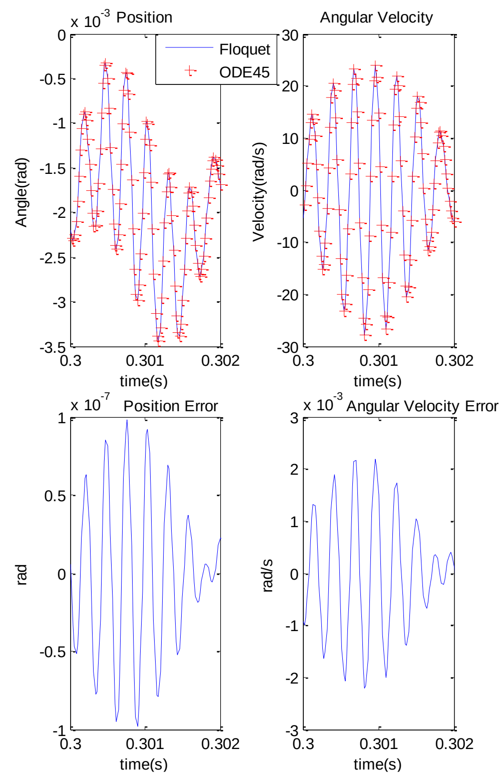


**Figure 6 System responses of θ4, ω(θ4) and their errors Error(θ4), Error[ω(θ4)] under 0 RPM**

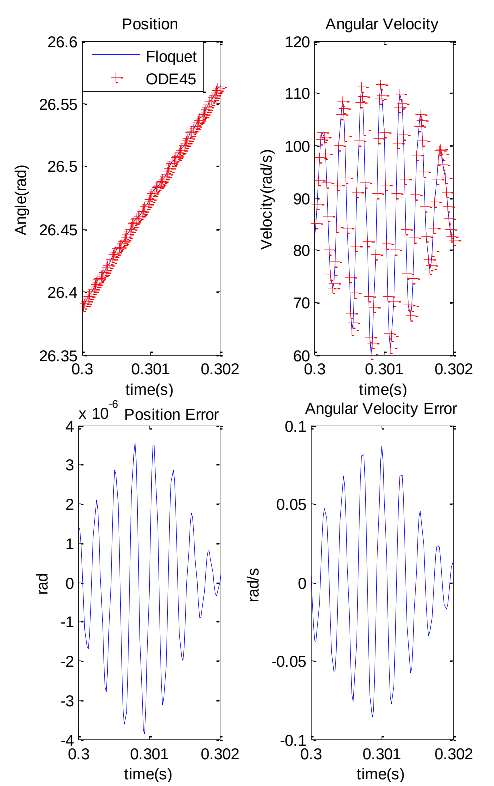


**Figure 7 System responses of θ4, ω(θ4) and their errors Error(θ4), Error[ω(θ4)] under 2100 RPM**

To verify the Floquet theory approach, a simplified numerical example is conducted based on a 4-DOF gear system shown in Figure 5. The system responses $\theta_4$ with respect to various initial velocities are compared with the results from Matlab ODE45 solver (i.e., direct numeric integration). Errors are shown in Figure 6 and Figure 7.

The comparison shows that the results from the analytical and direct integration methods match very well with each other. This indicates that the Floquet theory can be applied to predict the system response of the gear system.

## Eigenvalue analysis

We now come back to the original system described by Eq.(1) and Eq.(4). The system equation can be represented in general as the form shown in Eq.(13). In the state-space format, we can write

$$\dot{\mathbf{y}} = \mathbf{A}\mathbf{y} + \mathbf{b} \tag{20}$$

where

$$\mathbf{y} = \begin{bmatrix} \mathbf{x}^T & \dot{\mathbf{x}}^T \end{bmatrix}^T$$

$$\mathbf{A} = \begin{bmatrix} \mathbf{0} & \mathbf{I} \\ \mathbf{-M^{-1}K} & \mathbf{-M^{-1}C} \end{bmatrix}$$

$$\mathbf{b} = \begin{bmatrix} \mathbf{0} \\ \mathbf{M^{-1}F} \end{bmatrix}$$

Matrix $\mathbf{A}$ is time-periodic because of the time-varying mesh stiffness. It can be expanded in terms of the Fourier series as $\mathbf{A} = \sum_{j=-n}^{n} \mathbf{A}_j e^{c_j it}$, where $\mathbf{A}_j$ is the Fourier coefficients and $c_j$ is the corresponding circular frequencies. Here we introduce the solution as $\mathbf{y} = \sum_{k=1}^{2N} \mathbf{u}_k(t) e^{\lambda_k t}$. According to the Floquet theory, the eigenvalue problem of this time-varying system becomes [23, 24],

$$\dot{\mathbf{u}}_k(t) + \left[\lambda_k \mathbf{I} - \mathbf{A}(t)\right]\mathbf{u}_k(t) = \mathbf{0} \tag{21}$$

where $\lambda_k = \alpha_k + \omega_k i$ is the complex Floquet exponents, and $\mathbf{u}_k(t) = \sum_{j=-n}^{n} \mathbf{u}_{k,j} e^{c_j it}$ is the corresponding periodic mode shapes. By performing the harmonic balance method (HBM), we can transform Eq.(21) into a time-invariant hyper-eigenvalue problem as shown below,

$$\left(\lambda_k \mathbf{I} - \begin{bmatrix} \ddots & & & \iddots \\ & \mathbf{A}_0 + ic_j\mathbf{I} & \mathbf{A}_{-1} & \mathbf{A}_{-2} \\ & \mathbf{A}_1 & \mathbf{A}_0 & \mathbf{A}_{-1} \\ & \mathbf{A}_2 & \mathbf{A}_1 & \mathbf{A}_0 - ic_j\mathbf{I} \\ \iddots & & & \ddots \end{bmatrix}\right) \begin{Bmatrix} \vdots \\ \mathbf{u}_{k,-1} \\ \mathbf{u}_{k,0} \\ \mathbf{u}_{k,+1} \\ \vdots \end{Bmatrix} = \begin{Bmatrix} \vdots \\ \mathbf{0} \\ \mathbf{0} \\ \mathbf{0} \\ \vdots \end{Bmatrix} \tag{22}$$

In this specific case, the hyper-eigenvalue is a 240x240 dimension problem.

After solving the hyper-eigenvalue problem shown in Eq.(22), a series of basis eigenvalues and redundant eigenvalues are obtained, which are then plotted in Figure 8 for the system shown in Figure 1 with the constant motor speed 1710 RPM. Here the mesh stiffness is assumed to be a sinusoidal function; therefore the simple approach outlined in the preceding section can no longer be applied. To highlight the capability of the approach to dealing with time-periodicity, the backlash and mesh damping are set to be zero. The results obtained are plotted in Figure 8.

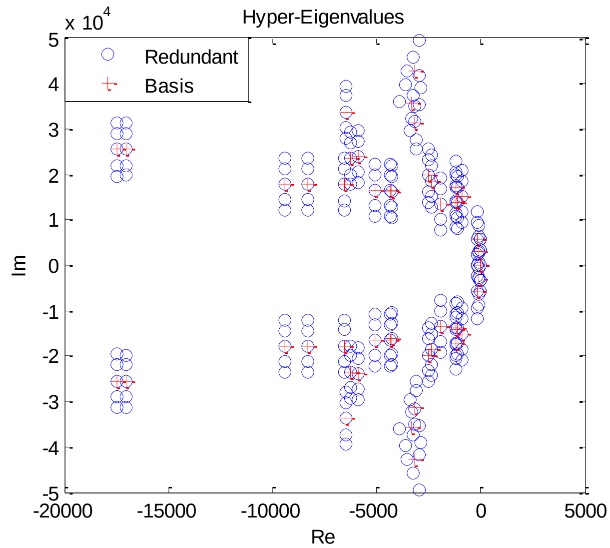

**Figure 8 Eigenvalues from hyper-problem**

Indeed, these eigenvalues characterize the dynamic features of the system responses. For example, the imaginary parts of these eigenvalues correspond to the resonant peaks in the frequency domain. Here we compare them with the results obtained by applying the Fast Fourier Transformation (FFT) to the numerical time domain system response. The frequencies calculated by means of the hyper-eigenvalues are plotted at the bottom of Figure 9 and Figure 10, where the red square indicates the basis component and the blue circle indicates the redundant component. In Figure 9, the results from the hyper-eigenvalues match very well with the basis frequencies located at 464.6Hz, 937.2Hz and 2401.6Hz. Similar observation can be obtained in Figure 10 at around 464.6Hz, 937.2Hz, 2401.6Hz, and 2939.7Hz. Further analysis reveals that the redundant frequencies around these basis ones are accurately reflected in sidebands given by the FFT results.

To analyze the gear system behavior under speed-varying operating condition, the motor speed profile is set to be time-varying as shown in Figure 11. The frequencies comparison shown in Figure 12 and Figure 13 indicates that the basis frequencies remain unchanged but the sidebands are speed dependent since the periodic parameter is directly related to the motor speed.

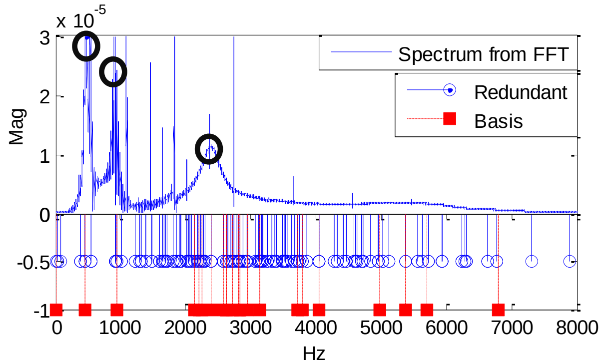

Figure 9 Frequencies comparison for ω(θ₁)

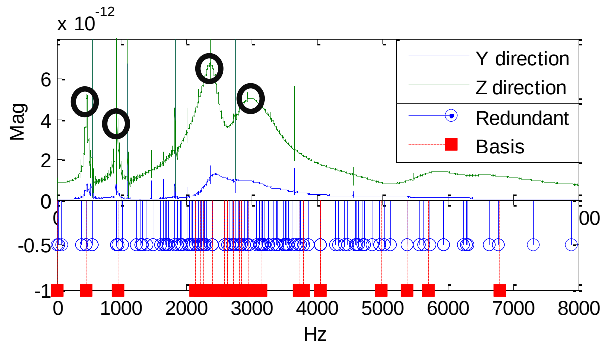

Figure 10 Frequencies comparison for Translation motion of Gear 2

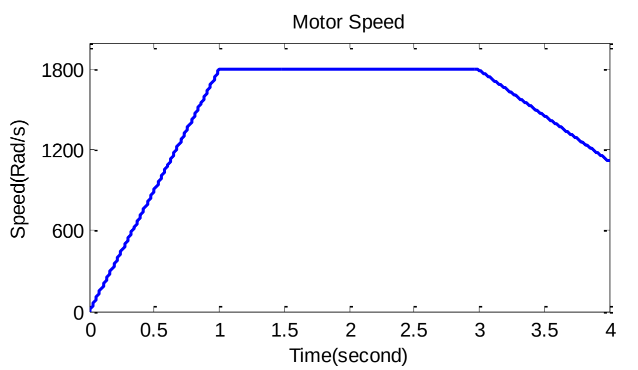

Figure 11 Time-varying speed profile of the motor

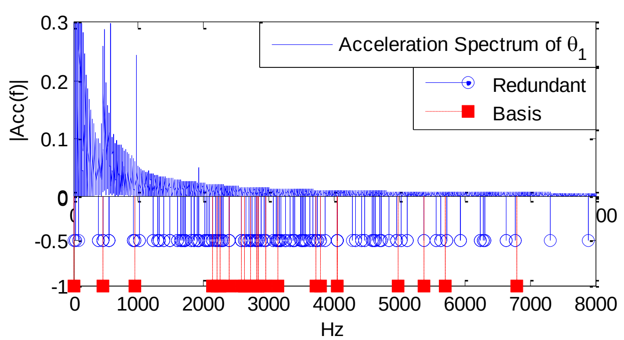

Figure 12 Frequencies comparison for a(θ₁) under time-varying speed

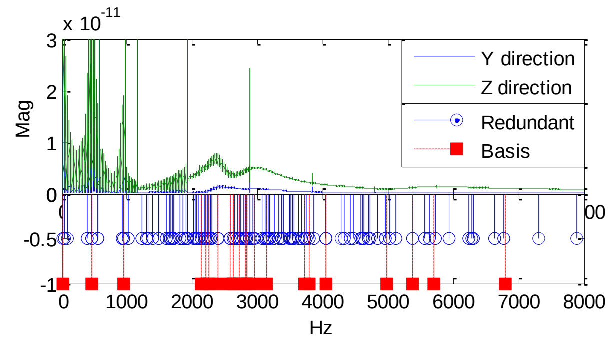

Figure 13 Frequencies comparison for translation motion of Gear 2 under time-varying speed

## CONCLUDING REMARKS

In this research, a mathematical model for a two-stage laboratory gearbox testbed is established by utilizing the assumed mode method (AMM). This modeling approach allows us to analyze gearbox responses over a wider frequency range. To analyze the time-varying periodic system, the Floquet theory and the harmonic balance method are employed simultaneously. This research extends such analysis from single-DOF case to multi-DOF case. Case studies indicate that the natural frequencies and frequency sidebands predicted by the hyper-eigenvalue problem match very well with the results obtained based on FFT of time-domain responses. This model and the associated analysis methods lay down a foundation for developing high-fidelity predictive modeling of gearbox systems. Future work will focus on the inclusion of nonlinear effects and the incorporation of experimental measurement data for parametric identification model updating.

## ACKNOWLEDGMENT

This research is supported by the National Science Foundation under grants CMMI-1300236 and CMMI-1300560.

## REFERENCES

[1] Hyers, R., McGowan, J., Sullivan, K., Manwell, J., and Syrett, B., 2006, "Condition monitoring and prognosis of utility scale wind turbines," Energy Materials: Materials Science and Engineering for Energy Systems, 1(3), pp. 187-203.

[2] Wilkinson, M. R., Spinato, F., and Tavner, P. J., "Condition monitoring of generators & other subassemblies in wind turbine drive trains," Proc. Diagnostics for Electric Machines, Power Electronics and Drives, 2007. SDEMPED 2007. IEEE International Symposium on, IEEE, pp. 388-392.

[3] Tavner, P. J., Bussel, G. J. W. v., and Spinato, F., 2006, "Machine and converter reliabilities in wind turbines," IET Conference Proceedings, Institution of Engineering and Technology, pp. 127-130.

[4] Lu, B., Li, Y., Wu, X., and Yang, Z., "A review of recent advances in wind turbine condition monitoring and fault

diagnosis," Proc. Power Electronics and Machines in Wind Applications, 2009. PEMWA 2009. IEEE, IEEE, pp. 1-7.
[5] Sheng, S., and Veers, P. S., 2011, Wind Turbine Drivetrain Condition Monitoring-An Overview, National Renewable Energy Laboratory.
[6] Randall, R. B., 2011, Vibration-based condition monitoring: industrial, aerospace and automotive applications, Wiley.
[7] Schlechtingen, M., Santos, I. F., and Achiche, S., 2012, "Wind turbine condition monitoring based on SCADA data using normal behavior models: Part 1–system description," Applied Soft Computing.
[8] Nevzat Özgüven, H., and Houser, D., 1988, "Mathematical models used in gear dynamics—a review," Journal of Sound and Vibration, 121(3), pp. 383-411.
[9] Theodossiades, S., and Natsiavas, S., 2000, "Non-linear dynamics of gear-pair systems with periodic stiffness and backlash," Journal of Sound and Vibration, 229(2), pp. 287-310.
[10] Wang, J., and Howard, I., 2004, "The torsional stiffness of involute spur gears," Proceedings of the Institution of Mechanical Engineers, Part C: Journal of Mechanical Engineering Science, 218(1), pp. 131-142.
[11] Özgüven, H., 1991, "A non-linear mathematical model for dynamic analysis of spur gears including shaft and bearing dynamics," Journal of sound and vibration, 145(2), pp. 239-260.
[12] Osman, T., and Velex, P., 2011, "A model for the simulation of the interactions between dynamic tooth loads and contact fatigue in spur gears," Tribology International.
[13] Vaishya, M., and Singh, R., 2001, "Analysis of periodically varying gear mesh systems with Coulomb friction using Floquet theory," Journal of Sound and Vibration, 243(3), pp. 525-545.
[14] Chaari, F., Fakhfakh, T., and Haddar, M., 2009, "Analytical modelling of spur gear tooth crack and influence on gearmesh stiffness," European Journal of Mechanics-A/Solids, 28(3), pp. 461-468.
[15] Vaishya, M., and Singh, R., 2003, "Strategies for modeling friction in gear dynamics," Journal of Mechanical Design, 125(2), pp. 383-393.
[16] Diehl, E. J., Tang, J., and DeSmidt, H., "Gear Fault Modeling and Vibration Response Analysis," Proc. ASME 2012 5th Annual Dynamic Systems and Control Conference joint with the JSME 2012 11th Motion and Vibration Conference, American Society of Mechanical Engineers, pp. 709-718.
[17] DeSmidt, H., Wang, K., and Smith, E., 2004, "Stability of a segmented supercritical driveline with non-constant velocity couplings subjected to misalignment and torque," Journal of sound and vibration, 277(4), pp. 895-918.
[18] Singh, R., 2008, "Dynamic transmission error prediction of helical gear pair under sliding friction using floquet theory," Journal of mechanical design, 130, pp. 052603-052601.
[19] Zhang, W., 1990, Rotor Dynamics Theory, Science Press.
[20] Comparin, R., and Singh, R., 1989, "Non-linear frequency response characteristics of an impact pair," Journal of sound and vibration, 134(2), pp. 259-290.
[21] Kiekbusch, T., Sappok, D., Sauer, B., and Howard, I., 2011, "Calculation of the Combined Torsional Mesh Stiffness of Spur Gears with Two-and Three-Dimensional Parametrical FE Models," Strojniški vestnik-Journal of Mechanical Engineering, 57(11), pp. 810-818.
[22] Kuang, J., and Yang, Y., 1992, "An estimate of mesh stiffness and load sharing ratio of a spur gear pair," Advancing power transmission into the 21 st century, pp. 1-9.
[23] Christensen, R. H., and Santos, I. F., 2005, "Modal controllability and observability of bladed disks and their dependency on the angular velocity," Journal of Vibration and Control, 11(6), pp. 801-828.
[24] Zhao, J., 2013, "Vibration based damage identification of time-varying dynamical systems," Doctor of Philosophy Dissertation, University of Tennessee.